Case Studies in Construction Materials 16 (2022) e00845

Contents lists available at ScienceDirect

Case Studies in Construction Materials

journal homepage: www.elsevier.com/locate/cscm

Enduring performance of alkali-activated mortars with metakaolin as granulated blast furnace slag replacement

Mohammad Ali Asaad [a], Ghasan Fahim Huseien [b,*], Ruhal Pervez Memon [c], S. K. Ghoshal [d,*], Hossein Mohammadhosseini [e], Rayed Alyousef [f,*]

[a] Department of Civil Engineering, Iraq University College (IUC), Basra, Iraq
[b] Department of Building, School of Design and Environment, National University of Singapore, Singapore 117566, Singapore
[c] Department Civil Engineering, Faculty of Engineering Science and Technology, Ziauddin University, Karachi 75000, Pakistan
[d] Department of Physics, AOMRG & Laser Centre, Faculty of Science, Universiti Teknologi Malaysia (UTM), Skudai 81310, Johor Bahru, Malaysia
[e] Institute for Smart Infrastructure and Innovative Construction (ISIIC), School of Civil Engineering, Universiti Teknologi Malaysia (UTM), Skudai 81310, Malaysia
[f] Department of Civil Engineering, Prince Sattam Bin Abdulaziz University, Al-Kharj 16273, Saudi Arabia

ARTICLE INFO

Keywords:
Alkali-activated binder
GBFS
MK
Drying shrinkage
Sulfuric acid resistance

ABSTRACT

In the construction industries worldwide, improving the materials durability and achieving sustainability are the main goal. Owing to their excellent strength performance various alkali-activated binders can be one of the alternative solutions to the polluting traditional cement. Currently, ground blast furnace slag (GBFS) is the major base material used in the alkali-activated binders. High drying shrinkage and low resistance to sulfuric acid attack affect negatively the durability performance and life span of alkali-activated paste, mortars, and concretes made from GBFS. Thus, a series of alkali-activated mortars (AAMs) were designed with various contents (5, 10, 15, 20 and 25, mass%) of metakaolin (MK) as GBFS replacement to improve their strength performance. In addition, the strength and durability performance of the designed mixes were compared with the control mixture prepared using 100% of GBFS. The impact of varying MK level on the long-term performance such as compressive strength, porosity, resistance to sulfuric acid attacks, wet-dry cycles, drying shrinkage, and carbonation were evaluated. Various recommended standards were followed to cast the specimens in different shapes (cubes, cylinders, and prisms) and sizes. Mortar containing 10% of MK as GBFS replacement showed the highest compressive strength (63.4 MPa) at 28 days of curing age. Furthermore, the inclusion of MK as GBFS replacement was shown to improve the AAMs durability performance wherein the drying shrinkage was reduced and the resistance to aggressive environments was increased. The specimens containing 5% and 10% of MK revealed a lower porosity and carbonation depth compared to the control specimen. It was concluded that the proposed AAMs due to their long-term stability can be the sustainable and potential substitutes to the traditional construction materials.

Abbreviations: AMMs, Alkali-activated mortars; GBFS, Ground blast furnace slag; OPC, Ordinary Portland Cement; MK, Metakaolin; HR, relative humidity; CS, Compressive strength; DS, Drying shrinkage; CD, Carbonation depth; P, Porosity; SEM, Scanning electronic microscopy; XRF, X-ray Fluorescence; XRD, X-ray diffraction; PSA, Particle size analyzer; UPV, Ultrasonic pulse velocity.

* Corresponding authors.
E-mail addresses: bdggfh@nus.edu.sg (G.F. Huseien), sibkrishna@utm.my (S.K. Ghoshal), r.alyousef@psau.edu.sa (R. Alyousef).

https://doi.org/10.1016/j.cscm.2021.e00845
Received 26 September 2021; Received in revised form 9 December 2021; Accepted 16 December 2021
Available online 18 December 2021

1. Introduction

Nowadays, the production of sustainable construction materials with high strength performance, excellent durability properties, and longer life span are the main goal for the industries. To meet the demanded of the construction sectors, several types of binders have constantly been developed for the sustainable pastes, mortars, and concretes. Meanwhile, GBFS based alkali-activated binders were introduced as high early strength construction materials with shorter setting time compared to the geopolymers (GPs) and traditional cement binders [1–4]. Till date, GBFS is mainly used to prepare AAMs due to its very high calcium content (40–55%) [5,6]. In the geopolymerization process, the inclusion of GBFS as the main part in alkali-activated binder was shown to impart CaO an ability to replace Na_2O in the formulation of dense (N-A-S-H) and C-(A)-S-H gels [7]. GBFS-based alkali-activated binder have several benefits such as easy curing at ambient temperatures [8], fast setting with very high early strength [9], and ability to prepare with low molarity of sodium hydroxide [10], and alkaline activator solution modulus [11]. Several studies [12–15] indicated the feasibility to achieve acceptable compressive strength (CS) using one-part alkaline activator solution. Considering these advantages of AAMs, they have been used in several construction applications including the repair materials, high strength mortars, and durable concrete [10,16–18].

Although alkali-activated binders have demonstrated more superior early strength properties in the building constructions compared to the geopolymer and traditional cement binders, their large-scale applications are still limited [19–21]. The volumetric instability and approximately two times higher drying shrinkage (DS) of AAMs than Ordinary Portland Cement (OPC) is the major problem for their widespread usage [22]. Some studies [23–26] reported that high CaO content in GBFS can negatively affect the AAMs performance by increasing the DS and reducing the resistance against sulfate and sulfuric acid attacks. In addition, high DS can induce a non-uniform deformation across the material to form tensile stresses, thus triggering harmful cracks formation. High DS of AAMs leads to more internal micro-cracks, thus affecting their overall performance [27]. These destructive cracks can create a pathway for various impurities to penetrate into the composites, severely destroying the load-bearing capacity and durability of concrete structures [28]. Previous studies [29–32] indicated that the DS characteristics of various alkali-activated composites are more complicated than OPC-based composites due to their complex hydration processes and shrinkage mechanisms. In recent years, various studies have been conducted to understand the DS behavior of AAMs useful for the development of shrinkage mitigating methods. However, all these studies remain relatively fragmented thereby lacking any classification for the shrinkage characteristics of AAMs. Amongst these AAMs, the shrinkage problem of alkali-activated slag (AAS) systems is particularly prominent, which is significantly higher than that of other alkali-activated composites made from fly ash (FA), metakaolin (MK), and coal gangue (CG) [33,34].

Several studies [25,35–37] examined the behavior of AAMs against aggressive environment such as sulfuric acid and sulfate solutions. It was reported that the deterioration of the alkali-activated binders can increase with the increase of GBFS levels in the alkali-activated matrix. One of the main mechanisms for such deterioration was argued to be the existence of high calcium contents in the concretes, mortars and pastes that cause acid attack and decalcification [15,16]. Decalcification is the dissolution and migration of calcium ions from the cement paste into the surrounding aggressive media [38–40]. Decalcification is also prevalent is AAMs due to their high calcium contents [41]. Komljenovic et al. [20] and Varga et al. [21] studied the decalcification mechanism in AAMs wherein ammonium nitrate was used for leaching the calcium ions. The results obtained from both studies revealed a superior decalcification resistance of AAMs compared to the OPC-based concretes. This observation was attributed to the absence of calcium hydroxide, a lower calcium to silicon ratio and higher level of polymerization of the silicate chains [20,21]. Furthermore, various slag sources were investigated and it was concluded that AAMs with a higher alumina content has longer chains, more intensely cross-linked, making them more stable and highly resistant against acid attack [21]. Shi [22] studied the performance of AAMs and PC paste after HNO_3 and CH3COOH acid exposure. It was found that after 580 days' of immersion in HNO_3 the AAMs and PC pastes were corroded to a depth of approximately 1 and 2.5 mm, respectively.

Davidovits [42] showed that the resistance of MK-based AAMs against acid corrosion (5% of H_2SO_4 and HCl) can be better than the normal cement specimens. Specimens prepared with OPC or GBFS/OPC mixture can easily deteriorate after the exposure to the acid solution. The estimated mass loss was observed in the range of 30–60% compared to 5–8% for the MK-based specimens. Muhammad et al. [43] studied the effect of MK contents on the strength and stability of some AAMs wherein their against sulfuric acid (H_2SO_4) solution exposure was assessed after 270 days of immersion. The results were compared with the control sample as well as specimens prepared with silica fumes (SFs), magnesium, and cement clinkers. Close visual inspection showed that AAMs specimens presented different levels of corrosion when the binder pastes were removed from the specimens' edges and surfaces. Mortar prepared with 1.5% of MK displayed a maximum washing out tendency of the binders or sand under the exposure that slowly decreased with the addition of MK up to 4.5%. The chemical reaction between alkali and MK (aluminosilicate precursors) produced GP [44,45]. The alkali-activated MK-based GP revealed high thermal stability compared to the traditional polymers-based materials and strength performance like cement. Currently, various AAMs in the construction sector became the green alternatives to OPC [46].

Materials containing appropriate ratios of silica and alumina when reacted with alkali (potassium and/ or sodium hydroxide) can form GP wherein the polymerization reaction enables to generate 3-dimensional alkali aluminosilicate gel binding aggregates. Although FA have been utilized widely in the AAMs-based products, MK is an emergent potential alternative material for the AAMs design [47]. MK is superior than FA due to the presence more consistent chemical components (SiO_2 and $Al_2O_3 \geq 90\%$) in MK. Thus, MK produces more reliable, consistent, and predictable construction materials effective for repairing applications. In fact, due to the lack of availability of FA in various nations their efficient uses for the production of blended cements and concretes have been deficient [48,49]. Consequently, the use of MK in combination with other alumina (Al_2O_3) and silica (SiO_2) enriched minerals are favorable for various practical applications [44].

In recent years, the design and characterizations of AAMs generated renewed interests for the understanding of complex geopolymerization mechanisms. Many studies revealed that the optimized AAMs-based products can achieve enhanced durability,

strength, and sustainability performances [50]. The structural development of sodium silicate incorporated slag-MK blends were studied and the impact of MK inclusion on the ultimate CS of the binders were determined [51]. The influence of various proportions of Al_2O_3 to SiO_2 on the setting times and hardening properties of some AAMs was evaluated [52]. Different ratios of Al_2O_3 to SiO_2 were shown to influence significantly the setting times and ultimate strength performance of the produced AAMs. Besides, the effect of various SiO_2 to Al_2O_3 ratios on the setting times, ultimate strength and workability of the designed AAMs was examined [53] wherein the SiO_2 to Al_2O_3 proportion in the range of 2.87–4.79 was found to be optimum.

In view of the potential of MK as an alternative material in the design of diverse AAMs, for the first time this paper examined the impact of MK on the long-term properties of some AAMs with MK as GBFS replacement. These AAMs were designed and systematically characterized to determine their potency as sustainable construction materials with improved stability against aggressive environment including H_2SO_4 attacks and lower DS. The impact of various MK contents (as the substitute of GBFS) on the early and late CS as well as the on the porosity was evaluated. DS performance of the produced AAMs at different curing ages was measured to determine the effect of MK inclusion in the alkali-activated matrix. In addition, the performance of the achieved AAMs against H_2SO_4 solution attack was assessed to measure their durability and corrosion resistance. Tests were conducted to assess the designed AAMs carbonation depth (CD) and resistance against wet-dry cycles. The results for the length change with time, residual CS, weight loss, and microstructures of the studied AAMs were analyzed, discussed, interpreted, validated with other findings, and compared with the control sample performance.

2. Methodology

2.1. Materials characterization

In this study, MK was used as the main source of Al_2O_3-SiO_2 to prepare AAMs. High purity Kaolin powder (whitish in color) of grade-KM40 was procured from a company located in Puchong (Selangor, Malaysia). Then, MK was synthesized using the earlier referred protocols wherein kaolin was dihydroxylated in a furnace before being calcined at 750 °C for 6 h [54], as shown in Fig. 1. The color of kaolin was altered from pure white to floral whitish after it was dehydroxylated. Pure GBFS (off-white in color) was obtained from Ipoh (Malaysia) and used as another resource material to prepare the proposed AAMs. Owing to both cementitious and pozzolanic characteristics GBFS is distinct from other auxiliary cementitious components, which builds up own hydraulic reaction when water is added to GBFS. The particles size of the calcined MK was measured using a particle size analyzer (PSA). The average particles size of the calcined MK and GBFS was 10 μm and 12.8 μm, respectively.

The scanning electronic microscope (SEM) was used to determine the morphology of GBFS and MK (size and shape of particles). The SEM image of GBFS (Fig. 2a) showed more uneven, nearly spherical, and angular-shaped particles with smoother surface compared to MK (Fig. 2b). The SEM images of MK revealed their irregular morphology (Fig. 2b) which consisted of highly disordered distribution of packed (in chunks or clusters) angular-shaped particles. These tiny chunks or lumps appeared as stacking layers of MK in the form of sheets.

Fig. 3 shows the X-ray diffraction (XRD) patterns of GBFS and MK (raw materials used to design AAMs) wherein MK displayed a halo in the range of 9.8–28° corresponding to the glassy phase and an intense Bragg's peak at 26.8° due to the crystalline structures of quartz (SiO_2), mullite ($Al_6Si_2O_{13}$), and alusite (Al_2SiO_3), magnesium silicate ($MgSiO_2$) and aluminum magnesium (AlMg). Muscovite

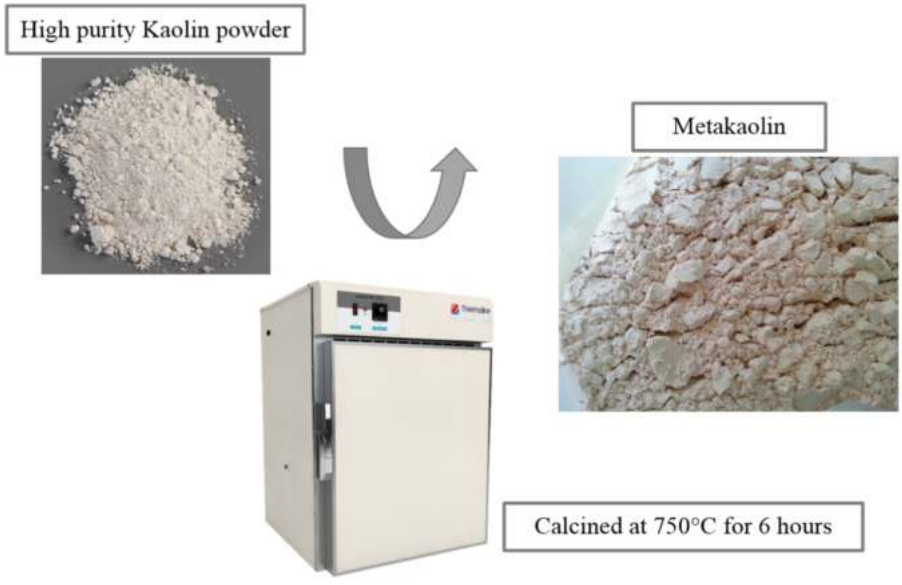

Fig. 1. Preparation stages of MK.

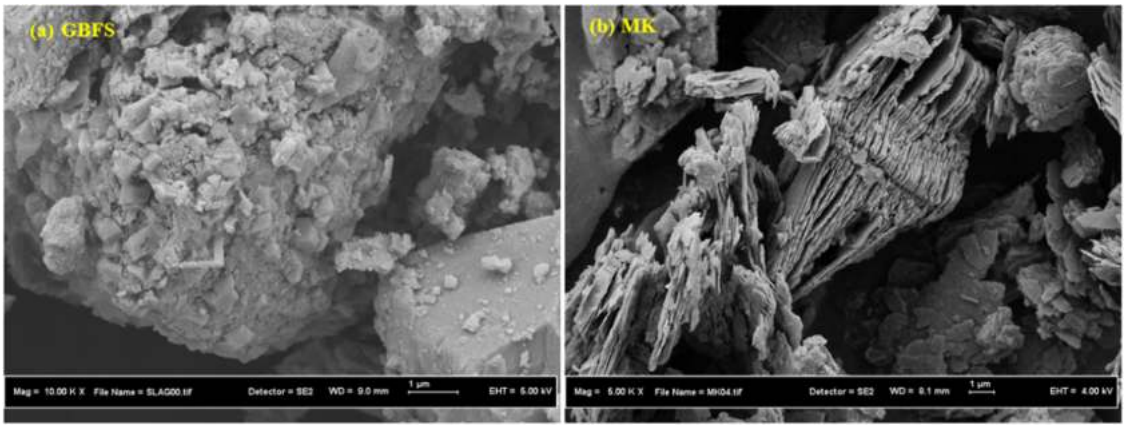

Fig. 2. Scanning electronic microscopy images of (a) GBFS and (b) MK.

($KAl_2(Si_3Al)O_{10}(OH.F)_{12}$) occurred as impurity from the resource constituents used for the AAMs preparation [54]. XRD profiles of GBFS showed largely the glassy phase with tiny quantity of magnetite crystallites [55].

The X-ray Fluorescence (XRF) spectra of GBFS and MK were recorded for determining their chemical composition (Table 1). The elemental analysis was performed using an energy dispersive X-ray spectrometer (Rigaku NEX-CG EDXRF). The results showed that silica and alumina oxides were the major composition of MK with 52.22% and 41.41%, respectively compared to the corresponding 30.53% and 13.67% observed with GBFS. The CaO content was found to be much lesser in MK (0.08%) compared to GBFS (46.02%). For this reason, MK was used as the main resource for silica and alumina and GBFS as major component for calcium in the preparation of AAMs. The presence of other components like iron, magnesium, potassium oxides were very low in the chemical composition of both materials. The loss on ignition (LOI) was found lower in GBFS chemical composition (0.22%) compared to MK (1.66%). MK meet the requirements (silica, alumina and iron oxides $\geq$ 85%) according to ASTM C618 standard [55].

The solutions of sodium hydroxide (NaOH of molar concentration 10) and sodium silicate (comprised of SiO_2, Na_2O and H_2O of 29.5, 14.70, and 55.80 mass%, respectively) were purchased from QREC (ASIA/Malaysia) and used as alkali activators. These solutions were utilized to activate the aluminosilicate during the geopolymerization process. NaOH with molar concentrations of 10 was considered for all the prepared mixtures. The mortars were prepared using the natural river sand (graded to ASTM C33) after oven drying at 60 °C for one day to control the moisture contents [56]. The aggregates' fineness modulus and specific gravity values were correspondingly 2.9 and 2.6. Super-plasticizer (SP) of Sika Visco Crete-3430 grade (kept constant to 3% of the binder) was used to enhance the workability of AAMs. The segregation tendency and uniformity of the mortars were controlled using the viscosity modifying admixtures (VMAs).

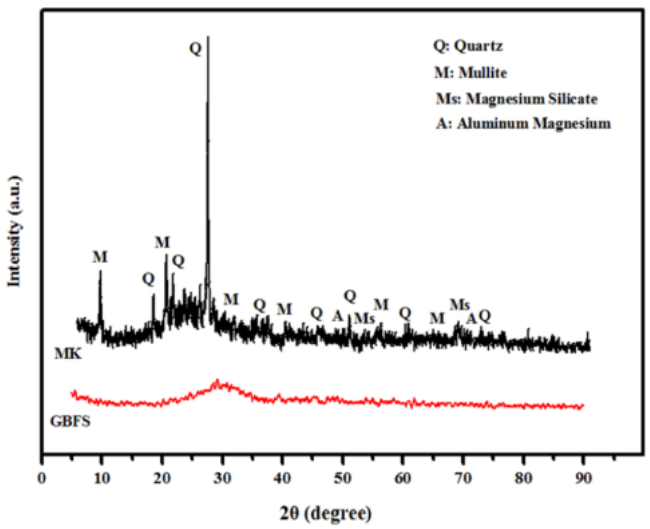

Fig. 3. GBFS and MK raw materials' XRD patterns.

Table 1
Occurrence of chemical constituents in GBFS and MK (mass%).

Elements	GBFS	MK
SiO_2	30.53	52.22
Al_2O_3	13.67	41.41
CaO	46.02	0.08
MgO	5.09	0.26
Fe_2O_3	0.33	0.49
Na_2O	0.24	0.01
K_2O	0.36	1.73
TiO_2	–	0.01
MnO	1.69	0.01
SO_3	1.35	1.92
LOI	0.22	1.66
Others	0.50	0.20

2.2. Mix design of AAMs

In this work, different proportions of GBFS and MK were blended to prepare the proposed AAMs. The mix designed using 100% of GBFS was considered as the control sample. Then, GBFS was replaced by various amounts of MK (5%, 10%, 15%, 20% and 25%) to examine their effect on the long-term properties of AAMs. It is well known that the substitution of GBFS by MK (containing very high amount the silica and alumina) can remarkably affect the ratio of calcium to silicate and calcium to alumina. Thus, these ratios were calculated to determine their effect on the durability performance, achieving the optimum level of replacement. The fixed values of other parameters for all mixes including the alkaline activator solution to binder (S:B), binder to fine aggregates (B:A), sodium silicate to sodium hydroxide (NS:NH), sodium hydroxide molarity, alkali-activator solution modulus (Ms) were correspondingly 0.40, 0.30, 2.5, 10 and 1.13. The specimens were designed by blending GBFS with MK over the duration of 3 min under dry state to get good homogeneity. Next, 50% of the fine aggregate was added and mixed for an additional 3 min. Later, the second part of fine aggregate was added and continued the mixing under drying condition for 3 min. Finally, the obtained mixture was alkali activated to get a homogeneous mortar mix for casting (in two layers with the compaction of each layer in the vibration table for 15 s) into cubical moulds of size 50 mm. After the casting, all the specimens were kept inside the moulds for 24 h before being opened and then cured at 27 °C with relative humidity of 75%. The early and late age strength and durability performance of the obtained mortars were evaluated. Table 2 shows the codes and composition of various designed mixes.

2.3. Tests

Following the ASTM C579 specification, the cubical moulds of size (50 mm × 50 mm × 50 mm) were made for testing the CS, porosity, wet-dry cycles, CD, and H_2SO_4 resistance. For the DS assessment, the prism shaped specimens of size (25 mm × 25 mm × 250 mm) were utilized. The CS test was performed for specimen adequately cured at 1, 7, 28, 56, 90, 180 and 360 days according to ASTM C109. For every curing age three sets of specimens were examined. The specimen under testing was made and placed precisely between the top and bottom metal-bearing plates as per the relevant specification. The load was applied at steady rate of 2.5 kN/s till the specimen failed. XRD being a rapid and simple technique for the non-destructive characterizations of the crystalline materials was used (Rigaku, SmartLab 3 kW) to determine the structures, phases and preferred crystal orientations of GBFS and MK. Fine powder of GBFS and MK was placed in the sample holder and then scanned at 2-theta vale in the range of 5–90° with scanning rate of 5°/min. The diffractometer operated at 30 mA/40 kV and used Cu K_α source of radiation wavelength (k) = 1.5406 Å. The surface morphology of AAMs was measured using a scanning electron microscope (HITACHI SU8020) with sufficient magnification. For the SEM imaging, each AAM after the CS test at 28 days of age was collected and then sowed onto double cellophane sheets followed by attachment to a coin. All specimens were coated in advance using a gold sputter coating machine.

The vacuum saturation method was utilized to evaluate the specimens' porosity following the ASTM C 642 standard. The specimens

Table 2
Codes and compositions of various designed mixes.

Materials (mass%) and ratios		Designed AAMs codes					
		AAM_1	AAM_2	AAM_3	AAM_4	AAM_5	AAM_6
Binder (B)	GBFS	100	95	90	85	80	75
	MK	0	5	10	15	20	25
	SiO_2:Al_2O_3	2.33	2.09	1.98	1.84	1.81	1.74
	CaO:SiO_2	1.51	1.38	1.26	1.15	1.05	0.96
	CaO:Al_2O_3	3.36	2.90	2.52	2.19	1.91	1.67
Solution to Binder (S:B)		0.40	0.40	0.40	0.40	0.40	0.40
Binder: Aggregate (B:A)		0.30	0.30	0.30	0.30	0.30	0.30
Na_2SiO_3:NaOH		2.5	2.5	2.5	2.5	2.5	2.5
Ratio of SiO_2:Na_2O (Ms)		1.13	1.13	1.13	1.13	1.13	1.13

under saturated, suspended, and oven-dried mass condition were used to obtain the appropriate properties. Cubical specimens with sufficient curing and saturated surface were tested at 28, 180 and 360 days. These cubic mortars were saturated in vacuum at respective ages and for each age, three specimens were used. The porosity (P in volume%) of the specimens was calculated via:

$$P = \left(\frac{ms - md}{ms - mb}\right) \times 100\% \quad (1)$$

where m_b, m_d, m_s are the sample's water-saturated buoyant mass, oven-dried mass at 105 °C, and air dried saturated surface mass.

The resistance of the mortars against the H_2SO_4 (10% from QREC, Malaysia) and sulfate ($MgSO_4$ of 10% from QREC, Malaysia) solution attacks were tested. Deionized water (DIW) was used to prepare the acid and sulfate solutions. After 28 days of curing age, twelve cubes were used to evaluate the mortars performance against the aggressive environments. First, the specimens were weighed prior to the immersion in the acid and sulfate solutions. During the entire test period, the specimens were closely monitored and the solutions were changed after every 3 months to maintain a constant pH level. After 6 and 12 months, the performance of AAMs were evaluated in terms of qualitative inspection, loss in strength, weight, and ultrasonic pulse velocity (UPV) based on ASTM C267 specifications. In the country like Malaysia that has rapidly fluctuating annual whether pattern (hot and dry for few days and then changes to rain for the next few days), no standard exists so far to study the specimens' resistance to wet-dry cycles. Based on this fact, this test is intended to mimic the Malaysian weather for accelerating the repeated wet-dry cycles. Fig. 4 shows the created wet-dry cycling state for the testing. The data was recorded in each 50 cycles and the effect of various dimension and mass on the residual strength was measured.

Following the ASTM C157/C157M specification, the DS test was carried out on 3 sets of prism shaped mortars of same size (25 mm × 25 mm × 250 mm). The test specimens were made according to ASTM C192/192 M stipulation and examined after curing at the ambient atmosphere. The specimens were embedded with stainless steel studs to measure the length changes. The mortars were de-mould after 24 h and transferred to a container kept at (23 ± 1) °C with relative humidity of (50 ± 5)%. Subsequently, the readings were taken using a demec meter at 3, 7, 14, 21, 28, 56, 90, 120, 180 and 360 days of curing age. Using the procedure recommended by BS 1881–210:2013, an accelerated CD test was performed within the chamber. The modified concrete specimens were exposed to a carbonated environment. This was carried out using a plastic container linked to a cylinder containing CO_2. The modified mortars contained in the plastic chamber were put into vacuum at 600 mm of mercury pressure under the relative humidity of 55–60% for three minutes. Then, the chamber was exposed to CO_2 at 26 °C for 28 and 180 days at the relative humidity of 4%. Between the gas chamber and plastic container a digitized pressure gauge was placed to monitor the pressure throughout the experiment. In this experiment, two cubical modified concrete specimens with the dimensions of (50 × 50 × 50) mm were observed. After 90 days in the gas cylinder, the mortars were cut in two pieces and the cross-sections were sprayed with a 0.2% phenolphthalein solution. Phenolphthalein turns non-carbonated concrete pink and remains colorless in carbonated concrete and the carbonation depth was thus determined.

3. Results and discussion

3.1. Compressive strength

The effects of various MK contents as GBFS replacement on the early and late strength of AAMs were evaluated (Fig. 5). The strength values were determined for age of 1, 7, 28, 56, 90, 180 and 360 days. The gain in compressive strength was monotonically

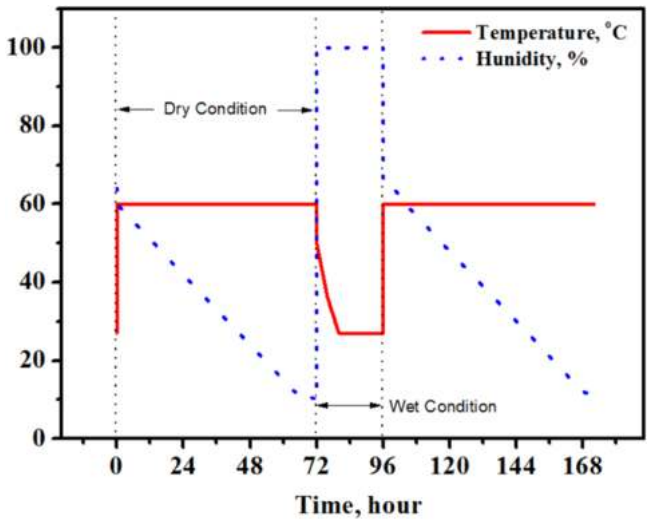

Fig. 4. Process for one wet-dry cycle.

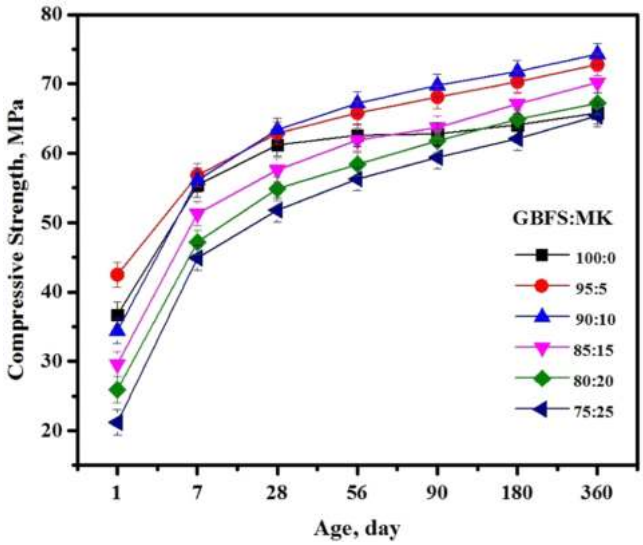

Fig. 5. Effect of MK as GBFS replacement on early and late CS development of the proposed AAMs.

increased with increasing age. At early age (1 day), the inclusion 5% of MK as GBFS replacement enabled to improve the CS to 42.5 MPa compared to the control sample (36.7 MPa). However, the increasing replacement level from 10% to 25% resulted in the reduction of the corresponding strength development from 34.4 to 21.2 MPa. Identical trends were shown by the mortars tested at 7 days of curing age and the highest CS (56.8 MPa) was recorded for the specimens designed with 5% of MK. It was found that an increase of MK content to 25% reduced the CS to 44.9 MPa compared to the control sample (55.4 MPa). Unlike, for the mortars cured at 28 days of age that contained 10% of MK presented the highest CS (63.4 MPa) compared to 61.2 and 62.9 MPa shown by the corresponding mortars made using 0% and 5% of MK. In addition, mortars tested at 56, 90, 180 and 360 days displayed similar trends. However, most of the MK-based mortars cured at 360 days of age exhibited an excellent performance with the strength value higher or closed to the control sample. The recorded CS for the specimens containing 0, 5%, 10%, 15%, 20% and 25% MK were 65.8, 72.8, 74.3, 70.2, 67.2 and 65.4 MPa, respectively.

In fact, the activation of two types of geopolymeric binders (one rich in calcium) in the mortars may present more advantages in terms of the condensation reaction acceleration than the one activated by the single calcium-free aluminosilicate [57,58]. It was found that [50] the replacement of 5% GBFS by MK could positively affect the strength performance due to the formulation of more dense gels. This result was mainly attributed to the increase of the curing age and complete geopolymerization reaction. With the increase of Al_2O_3 and SiO_2 contents in the mortars, the geopolymerization reaction was enhanced, producing more N-A-S-H and C-A-S-H gel in addition to the C-S-H and thus enhancing the strength properties of AAMs [59,60]. However, an increase of MK content up to 10% as replacement of GBFS was found to appreciably affect the amount of calcium oxide, thus limiting the C-(A)-S-H gels formation and leading to lower strength.

The SEM images in Fig. 6 display the effect of MK as GBFS replacement on the surface homogeneity and microstructures of the prepared AAMs. From Fig. 6a, it was observed that the degree of reaction in alkali-activated mix $AAMs_1$ is lower, leading to less dense

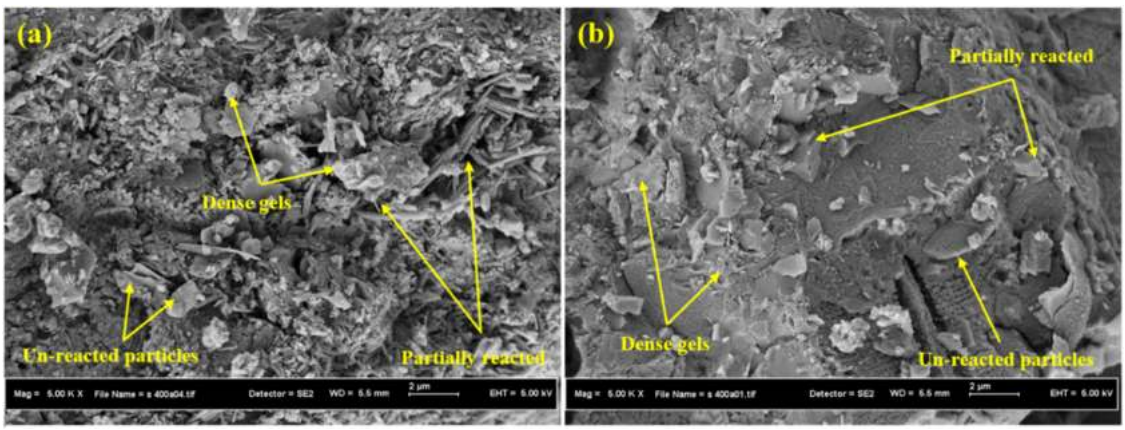

Fig. 6. SEM micrographs of AAMs prepared with (a) 0% and (b) 10% of MK.

gels with more voids. The inclusion of 10% MK as GBFS replacement in the alkali-activated matrix (Fig. 6b) was observed to improve the surface morphology compared to the control sample. Moreover, this polymerized binder was free of cracks along the interface at 10% of MK content. In addition, an increment in the alumina (Al_2O_3) content from 13.7% to 16.4% with increasing MK content from 0% to 10% led to enhance the geopolymerization process, producing extra dense gels. The reduction on $CaO:Al_2O_3$ ratio from 3.4 to 2.5 with increasing content of MK from 0% to 10%, contributed to increase the aluminum tobermorite ($Ca_2Al_2(SiO_2)(OH)_{10}.2.5(H_2O)$) and gmelinite ($Na_4(Si_8Al_4)O_{24}.11H_2O$) gels formulation. This shows that the geopolymerization reaction has taken place in alkali-activated mix $AAMs_3$ contributing to higher compressive strength. In previous studies [61–63] it was reported that the extra alumina and silica from the MK reacted with the Ca^{2+}in the GBFS to form the C-S-H and C-A-H gels. In addition, the fine particle size of MK filled the voids, decreasing the porosity of the mortars.

3.2. Porosity

Fig. 7 shows the porosity of AAMs at the curing ages of 28, 180 and 360 days as a function of MK to GBFS ratios. For all tested specimens, the porosity percentage was decreased with the increase of curing age. At 28 days, the increase of MK from 5% to 10% in place of GBFS reduced the porosity percentage of AAM from 6.1% to 5.5%, respectively. Unlike, the increase in the replacement level from 15% to 25% enabled to increase the corresponding porosity percentage from 6.4% to 6.9%. Analogous outcomes were obtained for the mortars tested at the curing age of 180 days wherein a lower porosity (4.7%) was achieved for the specimen made using 10% of MK compared to 5.4% obtained with control sample. After one year of the curing age, the results showed that an increase in the MK content from 0% to 25% led to an increase in the percentage of porosity from 5.3% to 5.4%, respectively. Specimens with higher contents of MK (up to 10%) revealed higher porosity which is mainly due to the generation of more gels. Very low content of Ca affected the silicate re-organization, thus lowering the C-A-S-H gel product and displaying poor structural homogeneity [64]. As the MK contents were increased from 10% to 25%, the degree of C-(A)-S-H gel formation was lowered, leading to the strength weakening and porosity enhancement. An increase in the silica and alumina contents up to an optimum ratio was shown to appreciably influence the number of partial and non-reacted particles responsible for the increase of AAMs porosity [65].

For AAMs containing high amount of MK (25%), such behavior may be due to presence of large amount of non-reacted silica particles in the specimen. It enhanced the AAMs porosity and water permeability through low Ca contents-enabled limited production of C-(A)-S-H gels compared to the control specimen [66–68]. Fig. 8 clearly showed the significant influence of AAMs porosity on their CS development. An inverse correlation between the CS and porosity of AAMs was evidenced. With the enhancement of the AAMs microstructures, the number of pores was reduced and thus lowering of porosity percentage. The following linear regression procedure was used to relate the experimental observation with $R^2 = 0.98$, indicating good confidence:

$$P = -0.1148CS + 12.936(\mathrm{R2} = 0.98) \quad (2)$$

3.3. Resistance against H_2SO_4 attack

One of the main objectives of this study was to enhance the AAMs durability against the aggressive or harsh environmental conditions including H_2SO_4 attack. For this purpose, the resistance of AAMs to acid attack was evaluated after 180 and 360 days. Quantities such as loss in the CS, weight, UVP, microstructures, and virtual appearance were examined. For all AAMs, the deteriorations were shown to increase with the increase of exposure times. The immersion of AAMs prepared with 5–25% of MK as GBFS replacement in the acid solution for 180 days was shown to enhance the durability performance and reduce the loss in strength from 42.3% to 29.7%, respectively (Fig. 9). Likewise, due to the inclusion of MK in the AAMs matrix the resistance of the tested specimens at

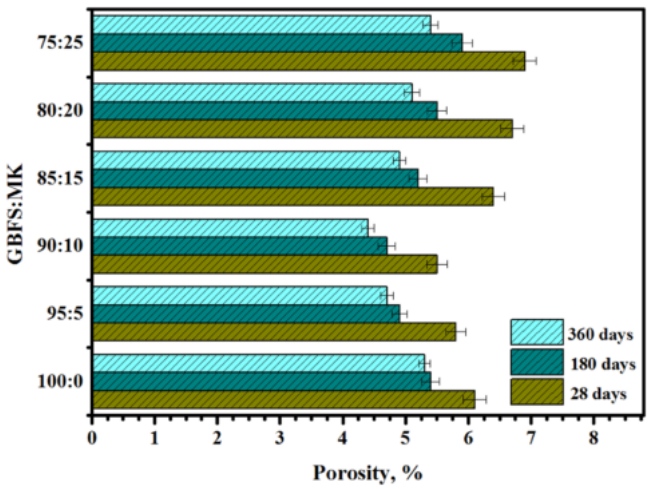

Fig. 7. Porosity of AAMs containing various amounts of MK as GBFS replacement.

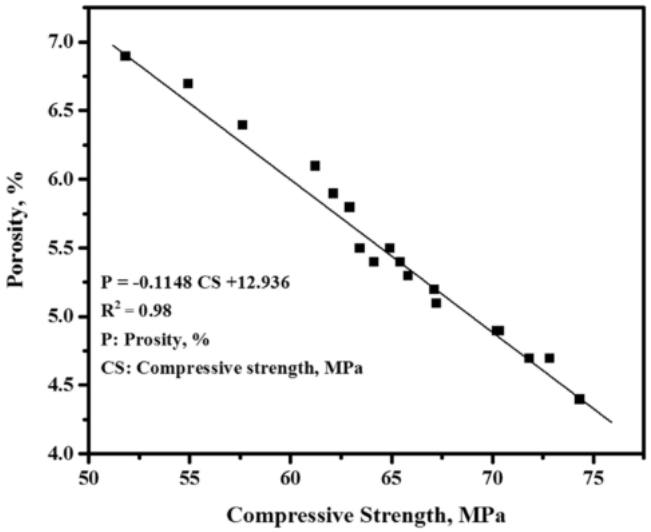

Fig. 8. Porosity and CS correlation in AAMs.

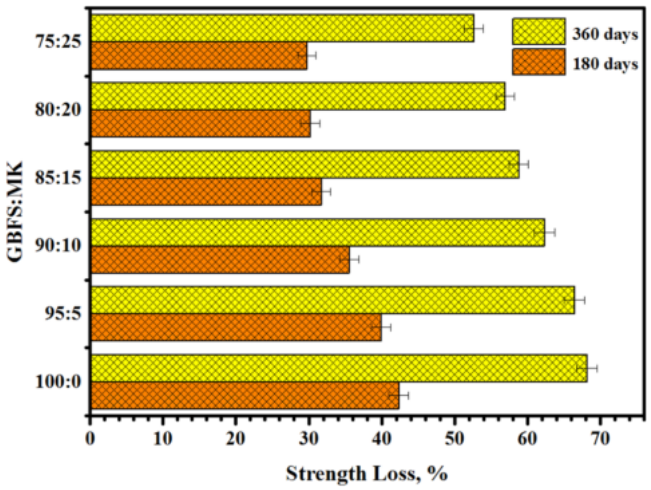

Fig. 9. Strength loss of the proposed AAMs under H_2SO_4 exposure.

360 days against acid attack was enhanced. The tendency of strength loss was dropped from 68.1% to 52.6% with corresponding increase of MK level from 0% to 25%. Regarding the weight loss of the AAMs, the inclusion of MK was found to reduce their deteriorations after exposed to acid solution attack (Fig. 10). At 180 days, the percentage weight loss was decreased from 1.56% to 1.03% with the increase of MK content from 5% to 25% as GBFS replacement, respectively. Equivalent trend was observed for the mortars after 360 days of acid exposure wherein the weight loss percentage was decreased from 2.46% to 1.98% with the corresponding increase of MK content from 0% to 25%.

The benefit of MK inclusion in AAMs in place of GBFS could restrict the gypsum formulation, thus reducing the internal cracks as evidenced from the UVP analyses (Fig. 11). At 180 days, the UPV readings were reduced from 10.9% to 8.1% with the corresponding increase of MK content from 0% to 25% as GBFS replacement. Specimens tested after 360 days exhibited higher deterioration compared to the one assessed at 180 days. Indeed, the inclusion of MK was shown to affect positively (enhancement) the mortars stability in sulfuric acid environment compared to the control sample (without MK and 100% of GBFS). The loss in the UPV reading was dropped from 21.7% to 12.9% with the corresponding increase of MK level from 5% to 25% as GBFS replacement.

Due to the exposure of H_2SO_4 solution, $Ca(OH)_2$ and SO_4^{-2} underwent strong reaction in AAMs matrix, producing gypsum ($CaSO_4.2H_2O$). The formation of gypsum allowed to expand the mortar's matrix, creating more cracks in the matrix and leading to additional corrosion of the mortar [69,70]. Compared to the blended mortars, the presence of high calcium content in the sample containing 100% of GBFS (control sample) produced higher amount of gypsum. Consequently, the mortar made with 25% of MK was the most resistant one against H_2SO_4 attack with CS loss below 29.7%. It was reported that [71] mortars (made from 100% of GBFS) activated with sodium silicate when exposed to acid solution could form large numbers of Ca^{++} and Na^{+} in the specimen matrix, thus

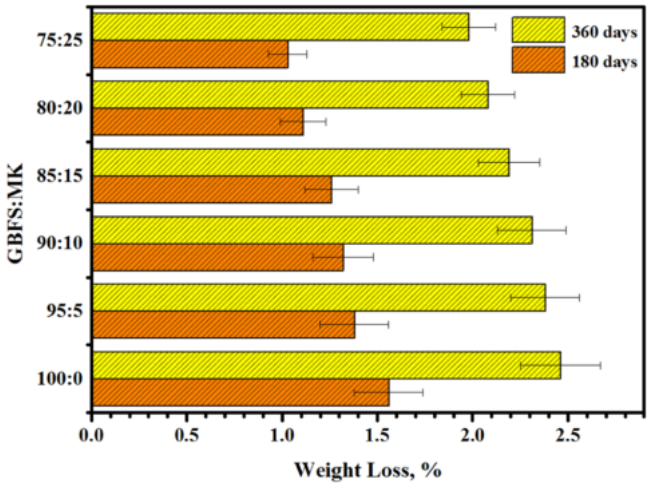

Fig. 10. Loss of weight of the proposed AAMs under H_2SO_4 exposure.

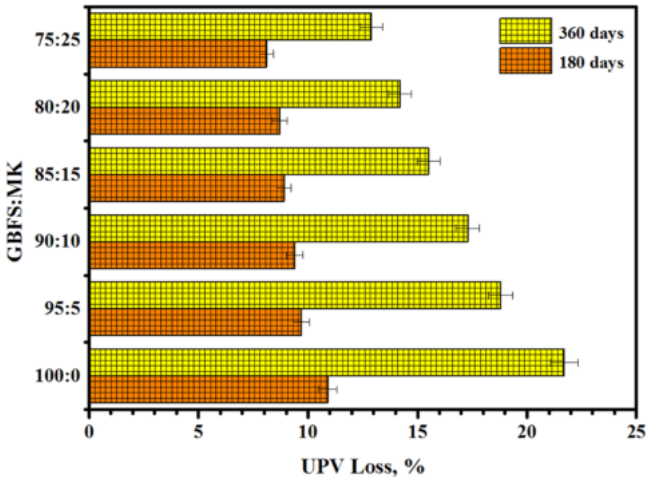

Fig. 11. UPV loss of the proposed AAMs under H_2SO_4 exposure.

achieving negative resistance to acid attacks. The exchange reactions among Ca^{++}, Na^{+} and OH^{-} caused an extra degradation of the gels and hence responsible for the CS loss. Furthermore, de-alumination was occurred because of the acid attack on the Si-O-Al linkages, producing significant structural alteration of the studied AAMs [72]. Several researchers [73–76] confirmed that with the increase of silica, alumina, and sodium levels the production of gypsum gets appreciably lowered, thus making the AAMs more durable.

3.4. Resistance to wet-dry cycles

The effect of MK as GBFS replacement on AAMs' resistance to wet-dry cycles was evaluated in term of the strength loss (Fig. 12). All the produced AAMs showed an increase in the CS loss with the increase of the wet-dry cycles. The specimens exposed to 150 wet-dry cycles revealed higher deterioration than the ones exposed to 50 and 100 cycles. The results showed that the inclusion of MK at 5% and 10% in the AAMs as GBFS replacement could appreciably enhance their durability and resistance to the wet-dry cycle. After 50 wet-dry cycles, the replacement of GBFS in AAMs by 5–10% of MK could reduce the corresponding CS loss from 1.22% to 0.96%. Likewise, the highest resistance after 100 wet-dry cycles was recorded for specimen containing 10% of MK which displayed loss in strength 2.91% compared to 3.62% for the control sample. After 150 wet-dry cycles, the recorded loss in strengths were 6.74%, 5.96%, 5.08%, 7.23%, 7.28% and 7.88% for AAMs designed with the MK contents of 0%, 5%, 10%, 15%, 20% and 25%, respectively.

The weight loss test was also adopted to evaluate the resistance of AAMs against wet-dry cycles (Fig. 13). All the specimens revealed an increase in the loss in weight with the increasing number of cycles. After 50 cycles, AAMs containing MK in place of GBFS was shown to produce very low percentage of weight loss. With the increase of MK level from 0% to 10% in AAMs could reduce their corresponding weight loss from 0.05% to 0.01%. However, an increase in the replacement level of MK in AAMs from 15% to 25% led to

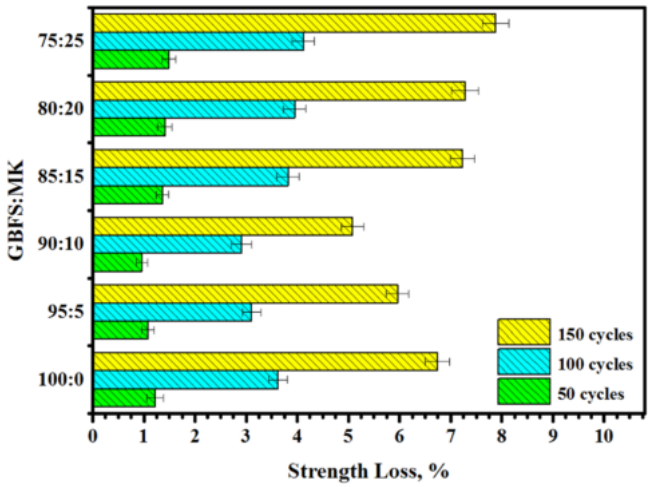

Fig. 12. Effect of MK content changes on AAMs' strength performance when exposed to wet-dry cycles.

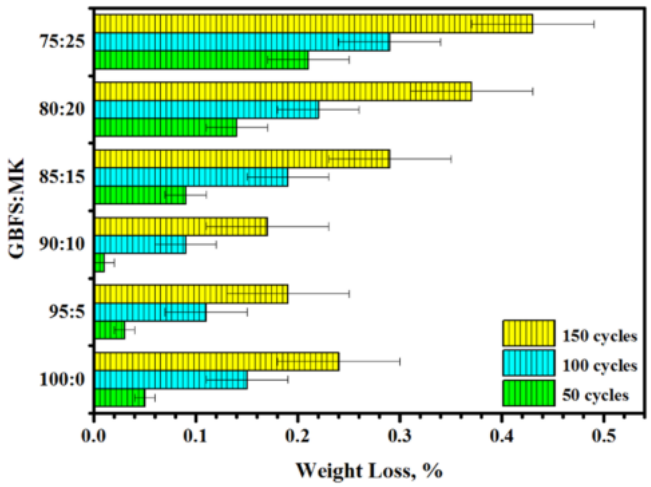

Fig. 13. Effect of MK content changes on AAMs' weight loss performance when exposed to wet-dry cycles.

an increase in the weight loss from 0.09% to 0.21%, respectively. Likewise, the specimen containing 10% of MK as GBFS replacement showed the highest resistance (0.09%) when exposed to 100 wet-dry cycles as opposed to the control sample (0.15%). Comparable results were obtained for the mortars tested after 150 cycles wherein the inclusion of MK as GBFS replacement by 5% and 10% could lower the corresponding weight loss percentage from 0.24% to 0.17%. Unlike, an increase in the GBFS replacement level from 15% to 25% by MK led to reduce the specimens' resistance and increase the corresponding weight loss from 0.29% to 0.43%. This observation can be ascribed to various factors. First, with the increase of mortars porosity the penetration depth and water level into the mortars matrix was enhanced during the wet-dry cycles, increasing the interior and exterior corrosion and thus lowering the long-term durability [77,78].

3.5. Drying shrinkage

The moisture movement and water loss due to evaporation caused the drying shrinkage (DS) in AAMs. The values of DS characterized the volume change of AAMs due to water evaporation. In aggressive environments, DS can cause the cracking of the binder matrix which in turn leads to an increased deterioration of mortars. Fig. 14 displays the benefits of MK inclusion in the AAMs as GBFS replacement in reducing the DS. The values of DS of the proposed mortars were increased with the increase of curing ages from 3 to 360 days. The results indicated that the inclusion of MK led to reduce the DS value at early and late age. Generally, the value of DS was increased with the increase of MK content. Specimen cured for 3 days with the replacement of 5–25% of GBFS by MK showed the corresponding drop of DS from 264.2 microstrain to 219.8 microstrain. Likewise, the value of DS at 360 days was lowered from 472.2 to 413.3 microstrain with the increase of corresponding MK level from 0% to 25%, thus improving the durability performance of

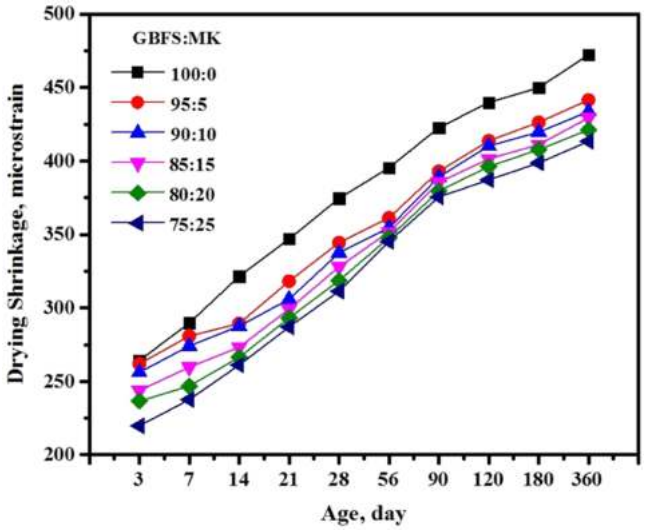

Fig. 14. Drying shrinkage of AAMs prepared with various ratio of GBFS to MK.

AAMs. The observed high DS value for GBFS-based AAMs was attributed to the creation of hydration products of the alkali-activate slag systems that consisted of C-(A)-S-H gel and silica rich gel containing a high amount of accumulated water [79,80]. It indicated the reduction in the shrinkage of drying specimens can be partly attributed to the lower amount of evaporable water as hydration and pozzolanic reaction used up significant amount of free water [81]. The higher value of DS of the specimens was mainly due to the evaporation of higher amount of un-combined water. The reduction of the relative humidity (HR) in the pore system could remove the moisture from the mesopores and lead to higher capillary stresses and higher surface tension, thus enhancing the drying shrinkage. These results were consistent with the previous studies [79,82–84] wherein it was indicated that the partial replacement of GBFS by materials with high silica and alumina content such SF, FA and POFA can effectively alleviate the DS of AAMs systems, weakening their strength development. Additionally, the incorporation of MK in AAMs was also an effective method in mitigating the autogenous and drying shrinkages [81,85]. The substitution of 10–20% of GBFS by MK was found to reduce the corresponding autogenous shrinkage of the alkali-activated pastes from 40% to 50% [86,87].

3.6. Carbonation depth (CD)

Fig. 15 displays the influence of various MK content as GBFS replacement on the carbonation depth of AAMs at 28 and 180 days. To determine the long-term stability of the proposed AAMs, they were exposed to CO_2 at early age (28 days) and late age (180 days) of curing. At early ages, the CD values of AAMs were dropped from 7.3 mm to 6.9 mm with the increase of MK level from 0% to 10%, respectively. Unlike, an increasing level of MK in AAMs from 15% to 25% could result in an increase of the corresponding CD value

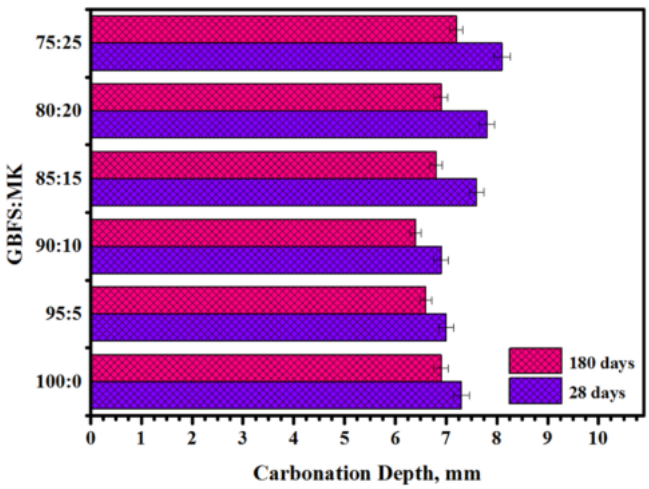

Fig. 15. Effect of MK content variation on carbonation depth of AAMs at 28 and 180 days.

from 7.6 to 8.1 mm. Comparable results were obtained for mortars tested at the late ages wherein the mortar made from 10% of MK as GBFS replacement showed the lowest depth of 6.4 mm. However, with the increase of MK content from 15% to 25% in the mortars, the CD was increased from 6.8 to 7.2 mm, respectively. This increase of CD was mainly due to the presence of isolated pores (not connected) in the mortar matrix which facilitated the admission of CO_2, thus lowering the emission level. According to Basheer et al. [88], the rate of CD increase of the mortars may be affected by various factors such as the porous networks' tortuosity, binding phases' chemistry, porous morphology and CO_2 transfer.

4. Conclusions

This paper determined the effect of various MK contents as GBFS replacement on the long-term performances of the proposed AAMs wherein the development of CS was assessed at various curing ages. Furthermore, the benefits of MK to enhance the durability performance of AAMs were evaluated in terms of the porosity, resistance to H_2SO_4 attack, we-dry cycles, DS and CD. Based on obtained results the following conclusions were drawn:

i. Incorporation of MK in place of GBFS in the AAMs led to produce high performance AAMs suitable for several applications in the construction sector.
ii. The highest CS (42.7 MPa) was achieved at early strength (3 days of curing age) for the AAM designed with 5% of MK as GBFS replacement. However, the AAM prepared with 10% of MK displayed the optimum strength at 28, 56, 90, 180 and 360 days of curing age. The replacement of GBFS by 5% and 10% of MK led to increase the silica and alumina in the mortar matrix, producing more gels and enhancing the strength performance.
iii. Replacement of GBFS by 10% of MK led to enhance the mortar's durability performance by reducing the porosity percentage at 28, 180 and 360 days compared to the control sample. The tested specimens revealed an inverse correlation between the CS and porosity.
iv. The resistance of AAMs to sulfuric acid attack was enhanced with the increase of MK contents. The specimens designed with 25% of MK yield lowest deterioration (in terms of strength, weight and UPV readings loss) after exposed to acid solution.
v. The inclusion of 10% of MK as GBFS replacement into the AAM was found to enhance the durability performance like resistance to wet-dry cycles. Specimens containing 10% of MK displayed the highest resistance against wet-dry cycles.
vi. The replacement of GBFS by MK in AAMs was demonstrated to be greatly advantageous solving the problem of high DS of GBFS. The early and late DS values of the proposed AAMs revealed a decreasing trend with the increase of MK content from 0% to 25%.
vii. The observed lower CD of the mortars containing 5% and 10% of MK as GBFS replacement than the control sample was mainly due to the enhanced and isolated porosity that facilitated the carbon dioxide penetration into higher depth.
viii. The attainment of high CS, low DS and high resistance against aggressive environments of the produced AAMs demonstrated their potential as perfect substitute to the traditional cement, leading to sustainable development of the construction industries.
ix. Compared to control specimens (100% GBFS), the modified mortars with MK as GBFS replacement shown excellent properties such as higher compressive strength, lower drying shrinkage and porosity, acidic resistant, devoid of emitting poisonous gases, energy production is low for building construction and several other industrial applications. Owing to these distinctive features, AAMs are potentially being employed in structure engineering, flame-retardant, bio-materials and waste management. New applications including the use of AAMs as concrete repair material for aggressive environments is under in-depth exploration.

Declaration of Competing Interest

The authors declare that they have no known competing financial interests or personal relationships that could have appeared to influence the work reported in this paper.

Acknowledgment

The authors gratefully acknowledge the support for this research from Ministry of Higher Education and Universiti Teknologi Malaysia Grant 16H94, Malaysia. Also, the authors gratefully acknowledge the support of Prince Sattam bin Abdulaziz University, Alkharj, Saudi Arabia.

References

[1] Z. Kubba, et al., Impact of curing temperatures and alkaline activators on compressive strength and porosity of ternary blended geopolymer mortars, Case Stud. Constr. Mater. 9 (2018), e00205.
[2] B.A. Salami, et al., Impact of Al (OH) 3 addition to POFA on the compressive strength of POFA alkali-activated mortar, Constr. Build. Mater. 190 (2018) 65–82.
[3] V. Lesovik, et al., Optimization of fresh properties and durability of the green gypsum-cement paste, Constr. Build. Mater. 287 (2021), 123035.
[4] A.R. de Azevedo, et al., Effect of the addition and processing of glass polishing waste on the durability of geopolymeric mortars, Case Stud. Constr. Mater. 15 (2021), e00662.
[5] A. Mehta, et al., Fly ash and ground granulated blast furnace slag-based alkali-activated concrete: Mechanical, transport and microstructural properties, Constr. Build. Mater. 257 (2020), 119548.
[6] A. Rafeet, et al., Effects of slag substitution on physical and mechanical properties of fly ash-based alkali activated binders (AABs), Cem. Concr. Res. 122 (2019) 118–135.

[7] K.W. Shah, G.F. Huseien, Bond strength performance of ceramic, fly ash and GBFS ternary wastes combined alkali-activated mortars exposed to aggressive environments, Constr. Build. Mater. 251 (2020), 119088.
[8] S. Kumar, R. Kumar, S. Mehrotra, Influence of granulated blast furnace slag on the reaction, structure and properties of fly ash based geopolymer, J. Mater. Sci. 45 (3) (2010) 607–615.
[9] H.K. Hamzah, et al., Strength performance of free cement mortars incorporating fly ash and slag: effects of alkaline activator solution dosage, Open J. Sci. Technol. 3 (2) (2020) 87–98.
[10] G.F. Huseien, A.R.M. Sam, R. Alyousef, Texture, morphology and strength performance of self-compacting alkali-activated concrete: Role of fly ash as GBFS replacement, Constr. Build. Mater. 270 (2021), 121368.
[11] H. Alabduljabbar, et al., Engineering properties of waste sawdust-based lightweight alkali-activated concrete: experimental assessment and numerical prediction, Materials 13 (23) (2020) 5490.
[12] B. Zhang, et al., Compressive stress-strain behavior of seawater coral aggregate concrete incorporating eco-efficient alkali-activated slag materials, Constr. Build. Mater. 299 (2021), 123886.
[13] T. Luukkonen, et al., One-part alkali-activated materials: a review, Cem. Concr. Res. 103 (2018) 21–34.
[14] T. Luukkonen, et al., Comparison of alkali and silica sources in one-part alkali-activated blast furnace slag mortar, J. Clean. Prod. 187 (2018) 171–179.
[15] M. Gonçalves, et al., Waste-based one-part alkali activated materials, Materials 14 (11) (2021) 2911.
[16] M. Wasim, T.D. Ngo, D. Law, Durability performance of reinforced waste-based geopolymer foam concrete under exposure to various corrosive environments, Case Stud. Constr. Mater. 15 (2021), e00703.
[17] I. Faridmehr, et al., Life-cycle assessment of alkali-activated materials incorporating industrial byproducts, Materials 14 (9) (2021) 2401.
[18] M. Samadi, et al., Influence of glass silica waste nano powder on the mechanical and microstructure properties of alkali-activated mortars, Nanomaterials 10 (2) (2020) 324.
[19] M.T. Marvila, et al., Mechanical, physical and durability properties of activated alkali cement based on blast furnace slag as a function of% Na2O, Case Stud. Constr. Mater. (2021), e00723.
[20] A. Azevedo, et al., Analysis of the compactness and properties of the hardened state of mortars with recycling of construction and demolition waste (CDW), J. Mater. Res. Technol. 9 (3) (2020) 5942–5952.
[21] B.C. Mendes, et al., Application of eco-friendly alternative activators in alkali-activated materials: a review, J. Build. Eng. (2020), 102010.
[22] M. Mastali, et al., Drying shrinkage in alkali-activated binders–a critical review, Constr. Build. Mater. 190 (2018) 533–550.
[23] G.F. Huseien, K.W. Shah, Durability and life cycle evaluation of self-compacting concrete containing fly ash as GBFS replacement with alkali activation, Constr. Build. Mater. 235 (2020), 117458.
[24] C. Grengg, et al., Deterioration mechanism of alkali-activated materials in sulfuric acid and the influence of Cu: a micro-to-nano structural, elemental and stable isotopic multi-proxy study, Cem. Concr. Res. 142 (2021), 106373.
[25] P. Sturm, et al., Sulfuric acid resistance of one-part alkali-activated mortars, Cem. Concr. Res. 109 (2018) 54–63.
[26] A. Azevedo, et al., Rheology, hydration, and microstructure of portland cement pastes produced with ground açaí fibers, Appl. Sci. 11 (7) (2021) 3036.
[27] G. Wang, Y. Ma, Drying shrinkage of alkali-activated fly ash/slag blended system, J. Sustain. Cem.-Based Mater. 7 (4) (2018) 203–213.
[28] A.R. de Azevedo, et al., Circular economy and durability in geopolymers ceramics pieces obtained from glass polishing waste, Int. J. Appl. Ceram. Technol. (2021).
[29] M. Hongqiang, et al., Study on the drying shrinkage of alkali-activated coal gangue-slag mortar and its mechanisms, Constr. Build. Mater. 225 (2019) 204–213.
[30] A.M. Rashad, A comprehensive overview about the influence of different admixtures and additives on the properties of alkali-activated fly ash, Mater. Des. 53 (2014) 1005–1025.
[31] R. Thomas, D. Lezama, S. Peethamparan, On drying shrinkage in alkali-activated concrete: Improving dimensional stability by aging or heat-curing, Cem. Concr. Res. 91 (2017) 13–23.
[32] M.T. Marvila, A.R.Gd Azevedo, C.M.F. Vieira, Reaction mechanisms of alkali-activated materials, Rev. IBRACON Estrut. Mater. (2021) 14.
[33] M.H. Al-Majidi, et al., Development of geopolymer mortar under ambient temperature for in situ applications, Constr. Build. Mater. 120 (2016) 198–211.
[34] I. Faridmehr, G. Fahim Huseien, M. Hajmohammadian Baghban, Evaluation of mechanical and environmental properties of engineered alkali-activated green mortar, Materials 13 (18) (2020) 4098.
[35] J. Zhang, et al., Durability of alkali-activated materials in aggressive environments: a review on recent studies, Constr. Build. Mater. 152 (2017) 598–613.
[36] N. Lee, H.-K. Lee, Influence of the slag content on the chloride and sulfuric acid resistances of alkali-activated fly ash/slag paste, Cem. Concr. Compos. 72 (2016) 168–179.
[37] A. Carvalho, et al., Environmental durability of soil-cement block incorporated with ornamental stone waste, Mater. Sci. Forum (2014).
[38] A.R. de Azevedo, et al., Investigation of the potential use of curauá fiber for reinforcing mortars, Fibers 8 (11) (2020) 69.
[39] M.T. Marvila, et al., Rheological and the fresh state properties of alkali-activated mortars by blast furnace slag, Materials 14 (8) (2021) 2069.
[40] A.R. de Azevedo, et al., Natural fibers as an alternative to synthetic fibers in reinforcement of geopolymer matrices: a comparative review, Polymers 13 (15) (2021) 2493.
[41] A.R. de Azevedo, et al., Use of glass polishing waste in the development of ecological ceramic roof tiles by the geopolymerization process, Int. J. Appl. Ceram. Technol. 17 (6) (2020) 2649–2658.
[42] Davidovits, J. Properties of geopolymer cements. in First international conference on alkaline cements and concretes. 1994. Kiev State Technical University, Ukraine: Scientific Research Institute on ….
[43] M.R. Ahmad, B. Chen, S.F.A. Shah, Influence of different admixtures on the mechanical and durability properties of one-part alkali-activated mortars, Constr. Build. Mater. 265 (2020), 120320.
[44] Z. Zhang, et al., Geopolymer from kaolin in China: an overview, Appl. Clay Sci. 119 (2016) 31–41.
[45] M.T. Marvila, et al., Performance of geopolymer tiles in high temperature and saturation conditions, Constr. Build. Mater. 286 (2021), 122994.
[46] P. Duxson, et al., The role of inorganic polymer technology in the development of 'green concrete', Cem. Concr. Res. 37 (12) (2007) 1590–1597.
[47] L. Chen, et al., Preparation and properties of alkali activated metakaolin-based geopolymer, Materials 9 (9) (2016) 767.
[48] V.M. Malhotra, P.K. Mehta, Pozzolanic and Cementitious Materials, Vol. 1, Taylor & Francis,, 1996.
[49] B. Sabir, S. Wild, J. Bai, Metakaolin and calcined clays as pozzolans for concrete: a review, Cem. Concr. Compos. 23 (6) (2001) 441–454.
[50] G.F. Huseien, et al., Effect of metakaolin replaced granulated blast furnace slag on fresh and early strength properties of geopolymer mortar, Ain Shams Eng. J. 9 (4) (2018) 1557–1566.
[51] S.A. Bernal, et al., Evolution of binder structure in sodium silicate-activated slag-metakaolin blends, Cem. Concr. Compos. 33 (1) (2011) 46–54.
[52] P. De Silva, K. Sagoe-Crenstil, The effect of Al 2 O 3 and SiO 2 on setting and hardening of Na 2 O–Al 2 O 3–SiO 2–H 2 O geopolymer systems, J. Aust. Ceram. Soc. 44 (1) (2008) 39–46.
[53] P. Chindaprasirt, et al., Effect of SiO2 and Al2O3 on the setting and hardening of high calcium fly ash-based geopolymer systems, J. Mater. Sci. 47 (12) (2012) 4876–4883.
[54] M. Ismail, et al., Early strength characteristics of palm oil fuel ash and metakaolin blended geopolymer mortar. Advanced Materials Research, Trans Tech Publ, 2013.
[55] Astm, C., 618. Standard Specification for Fly Ash and Raw or Calcined Natural Pozzolan for Use as a Mineral Admixture in Portland Cement Concrete, 2003.
[56] Commitee, A., C09. ASTM C33–03, Standard Spesification for Concrete Agregates. 2003, ASTM International.
[57] P.H. Borges, et al., Performance of blended metakaolin/blastfurnace slag alkali-activated mortars, Cem. Concr. Compos. 71 (2016) 42–52.
[58] I. Faridmehr, et al., Assessment of mechanical properties and structural morphology of alkali-activated mortars with industrial waste materials, Sustainability 13 (4) (2021) 2062.

[59] K. Dombrowski, A. Buchwald, M. Weil, The influence of calcium content on the structure and thermal performance of fly ash based geopolymers, J. Mater. Sci. 42 (9) (2007) 3033–3043.
[60] G.F. Huseien, et al., Influence of different curing temperatures and alkali activators on properties of GBFS geopolymer mortars containing fly ash and palm-oil fuel ash, Constr. Build. Mater. 125 (2016) 1229–1240.
[61] A. Hasnaoui, E. Ghorbel, G. Wardeh, Effect of curing conditions on the performance of geopolymer concrete based on granulated blast furnace slag and metakaolin, J. Mater. Civ. Eng. 33 (3) (2021) 04020501.
[62] O. Ayeni, A.P. Onwualu, E. Boakye, Characterization and mechanical performance of metakaolin-based geopolymer for sustainable building applications, Constr. Build. Mater. 272 (2021), 121938.
[63] K. Chen, et al., Mechanical and durability properties of metakaolin blended with slag geopolymer mortars used for pavement repair, Constr. Build. Mater. 281 (2021), 122566.
[64] H.K. Hamzah, et al., Effect of waste glass bottles-derived nanopowder as slag replacement on mortars with alkali activation: durability characteristics, Case Stud. Constr. Mater. (2021), e00775.
[65] X. Gao, Q. Yu, H. Brouwers, Assessing the porosity and shrinkage of alkali activated slag-fly ash composites designed applying a packing model, Constr. Build. Mater. 119 (2016) 175–184.
[66] G. Villain, M. Thiery, G. Platret, Measurement methods of carbonation profiles in concrete: Thermogravimetry, chemical analysis and gammadensimetry, Cem. Concr. Res. 37 (8) (2007) 1182–1192.
[67] A. Morandeau, M. Thiery, P. Dangla, Investigation of the carbonation mechanism of CH and CSH in terms of kinetics, microstructure changes and moisture properties, Cem. Concr. Res. 56 (2014) 153–170.
[68] G.F. Huseien, et al., Compressive strength and microstructure of assorted wastes incorporated geopolymer mortars: effect of solution molarity, Alex. Eng. J. 57 (4) (2018) 3375–3386.
[69] W. Zhang, et al., The degradation mechanisms of alkali-activated fly ash/slag blend cements exposed to sulphuric acid, Constr. Build. Mater. 186 (2018) 1177–1187.
[70] G.F. Huseien, et al., Evaluation of alkali-activated mortars containing high volume waste ceramic powder and fly ash replacing GBFS, Constr. Build. Mater. 210 (2019) 78–92.
[71] A. Allahverdi, F. Skvara, Sulfuric acid attack on hardened paste of geopolymer cements-Part 1. Mechanism of corrosion at relatively high concentrations, Ceram. Silik. 49 (4) (2005) 225.
[72] L. Gu, T. Bennett, P. Visintin, Sulphuric acid exposure of conventional concrete and alkali-activated concrete: assessment of test methodologies, Constr. Build. Mater. 197 (2019) 681–692.
[73] M.A.B. Ahmed, et al., Performance of high strength POFA concrete in acidic environment, Concr. Res. Lett. 1 (1) (2010) 14–18.
[74] M. Ariffin, et al., Sulfuric acid resistance of blended ash geopolymer concrete, Constr. Build. Mater. 43 (2013) 80–86.
[75] S. Bamaga, et al., Evaluation of sulfate resistance of mortar containing palm oil fuel ash from different sources, Arab. J. Sci. Eng. 38 (9) (2013) 2293–2301.
[76] A. Noruzman, et al., Strength and durability characteristics of polymer modified concrete incorporating Vinyl acetate effluent. Advanced Materials Research, Trans Tech Publ.,, 2013.
[77] H. Chang, et al., Influence of pore structure and moisture distribution on chloride “maximum phenomenon” in surface layer of specimens exposed to cyclic drying-wetting condition, Constr. Build. Mater. 131 (2017) 16–30.
[78] G.F. Huseien, et al., The effect of sodium hydroxide molarity and other parameters on water absorption of geopolymer mortars, Indian J. Sci. Technol. 9 (48) (2016) 1–7.
[79] A.M. Humad, et al., The effect of blast furnace slag/fly ash ratio on setting, strength, and shrinkage of alkali-activated pastes and concretes, Front. Mater. 6 (2019) 9.
[80] G. Huseien, et al., Performance of sustainable alkali activated mortars containing solid waste ceramic powder, Chem. Eng. Trans. 63 (2018) 673–678.
[81] J. Brooks, M.M. Johari, Effect of metakaolin on creep and shrinkage of concrete, Cem. Concr. Compos. 23 (6) (2001) 495–502.
[82] Z. Li, et al., Prediction of the autogenous shrinkage and microcracking of alkali-activated slag and fly ash concrete, Cem. Concr. Compos. 117 (2021), 103913.
[83] Gong, J. and Z. Qu, Mechanical Properties and Drying Shrinkage Investigation of Alkali-Activated Mortar Using Waste Glass Powder. Advances in Civil Engineering, 2020. 2020.
[84] G.F. Huseien, K.W. Shah, Performance evaluation of alkali-activated mortars containing industrial wastes as surface repair materials, J. Build. Eng. 30 (2020), 101234.
[85] M.R. Schuab, W.J. dos Santos, P.H.R. Borges, On the development of MK/BFS alkali-activated materials as repair mortars: performance under free and restrained shrinkage tests, Constr. Build. Mater. 275 (2021), 122109.
[86] Z. Li, et al., Mitigating the autogenous shrinkage of alkali-activated slag by metakaolin, Cem. Concr. Res. 122 (2019) 30–41.
[87] G.F. Huseien, et al., Geopolymer mortars as sustainable repair material: a comprehensive review, Renew. Sustain. Energy Rev. 80 (2017) 54–74.
[88] L. Basheer, J. Kropp, D.J. Cleland, Assessment of the durability of concrete from its permeation properties: a review, Constr. Build. Mater. 15 (2–3) (2001) 93–103.